arXiv:1011.6345v4 [cond-mat.stat-mech] 24 Jun 2011

Non-Fickian Diffusion and the Accumulation of Methane Bubbles in Deep-Water Sediments

D. S. Goldobin,[1,3] N. V. Brilliantov,[1] J. Levesley,[1] M. A. Lovell,[2] C. A. Rochelle,[4]
P. D. Jackson,[4] A. M. Haywood,[5] S. J. Hunter,[5] and J. G. Rees[4]

In the absence of fractures, methane bubbles in deep-water sediments are immovably trapped within a porous matrix by surface tension. The dominant mechanism of transfer of gas mass therefore becomes the diffusion of gas molecules through porewater. The accurate description of this process requires non-Fickian diffusion to be accounted for, including both thermodiffusion and gravitational action. We evaluate the diffusive flux of aqueous methane considering non-Fickian diffusion and predict the existence of bubble mass accumulation zones within deep-water sediments. The occurrence of these may be highly significant in the assessment of methane hydrate reservoirs or inventories as they could occur independently of the hydrate stability zone, yet may mimic the bottom-simulating-reflector which is commonly used to identify the base of the zone.

1. Introduction

The occurrence of methane bubbles within porous water-saturated sediments is widespread around the ocean margins. The gas within them plays an important role in both submarine hazards, such as submarine landslides [*Kayen and Lee*, 1991] as well as the formation of resources, such as methane-hydrate deposits [*Davie and Buffett*, 2001, 2003; *Archer*, 2007]. The stability of the bubbles has a significant control on the methane flux from the sediments into the ocean-atmosphere system.

In porous sediments the bubbles are trapped within the matrix pores. Large moving bubbles are unstable, as they split into smaller bubbles during migration [*Lyubimov et al.*, 2009; *Barry et al.*, 2010], and smaller bubbles are trapped by pore-throats or by surface tension forces. The minimum pore throat diameter l required to trap a small bubble, when there is no strong pumping of the fluid through the porous matrix, can be calculated. The surface tension forces σl (σ is the surface tension) should overwhelm the buoyancy force $\rho g l^3$ (ρ is the density, g is the gravity), i.e., $l < \sqrt{\sigma/\rho g}$. For gas-water systems, one finds, $l < [0.073\,N\,m^{-1}/10^3 kg\,m^{-3}\,9.8\,m\,s^{-2}]^{1/2} \approx 2.7\,mm$. Making allowance for the inhomogeneity of pores and the geometry of contacts, one should decrease this estimate to $l \approx 1\,mm$, which still suggests trapping even for sands. For a soft mud, mechanics of bubbles and porous matrix can be different [*Algar et al.*, 2011] and is not considered here.

As bubbles are trapped, and in the absence of significant groundwater movement transporting dissolved methane, the dominant mechanism of methane mass transfer in deep-water sediment is by diffusion of methane through porewater, controlled by (i) the methane saturation of the aqueous solution throughout the sediment volume, and (ii) non-Fickian diffusion laws. The latter pertain to two processes: firstly, the geothermal gradient causes thermodiffusion (the Soret effect [*Sorét*, 1879]), where the temperature gradient induces solute flux (as recognized in several fields, e.g. [*Richter*, 1972]); and secondly, the impact of gravity on dissolved molecules. These non-Fickian contributions to the diffusive flux mean that the solute flux cannot solely be determined by the gradient of the solute concentration.

Currently non-Fickian diffusion is rarely considered in the modelling of deep-water sediment systems (*Davie and Buffett* [2001, 2003]; *Haacke et al.* [2008]; *Garg et al.* [2008], and others involved in gas hydrate modelling only address Fickian diffusion). However, we suggest that non-Fickian processes are important; whilst appearing counter-intuitive, they may cause methane to migrate against the direction of the steepest decrease of concentration under certain conditions. Unfortunately, the experimental value of the thermodiffusion coefficient for the aqueous methane solution is unknown and can only be roughly assessed theoretically. Therefore, we treat it as a free parameter in our investigation. This uncertainty also justifies the fact that prior numerical modelling work did not include non-Fickian processes.

In researching the horizontal through-flow of water and vertical aqueous oxygen transport in porous bubble-bearing sediments, *Donaldson et al.* [1997] considered the hydrodynamic dispersion (*or* "turbulent diffusion" [*Bernard and Wilhelm*, 1950]), caused by water transport through irregular pore channels, as a transport mechanism and reasonably neglected the molecular diffusion. Indeed, the turbulent diffusion plays a significant role in vertical dissolved gas transport near the earth's surface. However, it becomes insignificant away from the sediment-water interface in deep-water sediments, where vertical and horizontal displacements of water are comparable. Here it is significantly smaller than molecular diffusion—even in sandy sediments.

In the present study we consider the diffusive migration of methane in sea-floor sediments where water is saturated with methane, and some methane is gaseous (forming bubbles; see sketches in Fig. 1). To evaluate the solubility and diffusive flux of methane we employ the physical model developed by *Goldobin and Brilliantov* [2011] and summarized in the Appendix. We demonstrate that even in the presence of the advective transport by the upward fluid flux, the non-Fickain diffusion is still important.

---

[1]Department of Mathematics, University of Leicester, Leicester LE1 7RH, UK.

[2]Department of Geology, University of Leicester, Leicester LE1 7RH, UK.

[3]Institute of Continuous Media Mechanics, UB RAS, Perm 614013, Russia.

[4]British Geological Survey, Keyworth, Nottingham NG12 5GG, UK.

[5]School of Earth and Environment, University of Leeds, Leeds LS2 9JT, UK.

Copyright 2011 by the American Geophysical Union.
0094-8276/11/$5.00

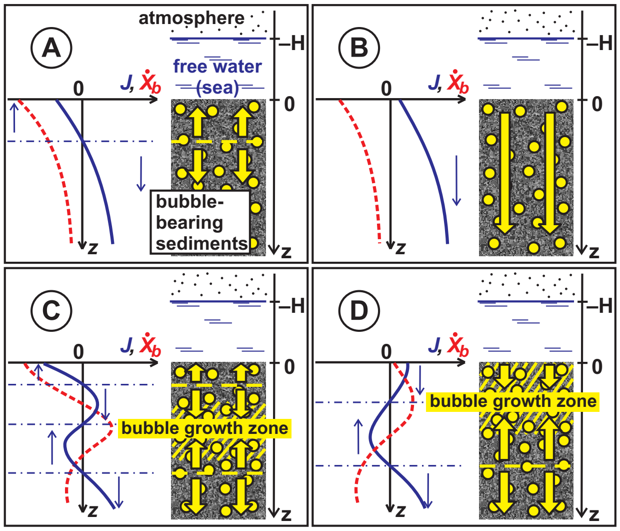

Figure 1. Four possible profiles of diffusive flux driven by the solubility profile and non-Fickian effects. The blue solid lines depict the flux J vs the depth below the water-sediment interface, z. The red dashed lines correspond to the free-gas production $\dot{X}_{\mathrm{b}}$, resulted from the diffusive flux J. In the diagrams the directions of fluxes and zones of methane accumulation from aqueous solution into free-gas bubbles (that is zones of positive $\dot{X}_{\mathrm{b}}$) are shown.

2. Diffusion in non-isothermal aqueous solutions bearing bubbles

Under non-isothermal conditions the diffusive flux of solute molar fraction X in the solvent is governed by the law (cf [*Bird et al.*, 2007; *Goldobin and Brilliantov*, 2011])

$$\vec{J}_{\mathrm{diff}} = -\phi D X \left[\frac{\nabla X}{X} + \alpha \frac{\nabla T}{T} - \frac{\tilde{M}\vec{g}}{RT} \right]. \qquad (1)$$

Here D is the solute effective molecular diffusion coefficient, ϕ is the porosity of the solid matrix. The first term describes the "ordinary" Fickian diffusion, $\vec{J}_{\mathrm{Fick}} = -\phi D \nabla X$. The second term represents the thermodiffusion effect appearing in non-isothermal systems, where temperature inhomogeneity causes a solute flux. The strength of the thermodiffusion effect is characterized by the thermodiffusion constant α (the conventional Soret *or* separation coefficient $S_T = \alpha/T$). The third term describes the action of gravity on solute molecules; $R = 8.31\,J/(mol\,K)$ is the universal gas constant, $\tilde{M} = M^{\mathrm{g}} - N_1 M^{\mathrm{host}}$, M^{g} and M^{host} are the molar masses of the solute and solvent, respectively, and N_1 is the number of solvent molecules in the volume occupied by one solute molecule in the solution. The value of N_1 can be precisely derived for CH_4–H_2O systems from the dependence of the solution density on its concentration [*Hnedkovsky et al.*, 1996]; one obtains $N_1 = 2.23$ and $\tilde{M} = -24.3\,g/mol$.

When the liquid is saturated with gas bubbles, the concentration of solute in solvent equals the solubility, $X = X^{(0)}$, throughout the liquid volume because the bubbles are in local thermodynamic equilibrium with the solution. Thus, the solute flux depends merely on the temperature and pressure fields, $T(z)$ and $P(z)$, and the solution concentration is not a free variable, $X(z) = X^{(0)}(T(z), P(z))$. For the calculation of the solubility see the Appendix.

In marine sediments, the processes of sediment compaction and related fluid advection can be important [*Davie and Buffett*, 2001, 2003]. With these processes, the solute flux reads

$$\vec{J} = \vec{J}_{\mathrm{diff}} + \vec{u}_{\mathrm{f}} X, \qquad (2)$$

where $\vec{u}_{\mathrm{f}}$ is the fluid filtration velocity, which is related to the interstitial fluid velocity $\vec{v}_{\mathrm{f}} = \vec{u}_{\mathrm{f}}/\phi(z)$.

Generally, the flux (2) possesses non-zero divergence $\nabla \cdot \vec{J}$, which requires sources and sinks of the solute mass—provided by bubbles. The mass production $(-\nabla \cdot \vec{J})$ is consumed by the bubble volume;

$$\phi \left[\frac{\partial X_{\mathrm{b}}}{\partial t} + \vec{v}_{\mathrm{s}} \cdot \nabla X_{\mathrm{b}} \right] = -\nabla \cdot \vec{J}, \qquad (3)$$

where X_{b} is the molar fraction of bubbles in the bubble-bearing fluid (comprising bubbles and liquid); $\vec{v}_{\mathrm{s}}$ is the velocity of sediments movement due to the compaction. By virtue of the mass conservation law for sediments, $v_{\mathrm{s}}(z) = ([1-\phi(0)]/[1-\phi(z)])v_{\mathrm{s}}(0)$ [*Davie and Buffett*, 2001].

3. Evolution of methane bubbles in the seabed

On the field scale, deep-water sediments are typically much more uniform horizontally rather than vertically. Consequently, we consider a system that is uniform horizontally. The depth below the seafloor is measured by the z-coordinate (Fig. 1). The system is essentially characterized by the hydrostatic pressure P and geothermal temperature gradient G;

$$P(z) = P_0 + \rho_{\mathrm{liq}} g (z + H), \qquad T(z) = T_{\mathrm{sf}} + Gz, \qquad (4)$$

where P_0 is the atmospheric pressure, H is the height of sea-water (water depth) above the bubble-bearing porous sediments, and T_{sf} is the temperature at the sediment-water interface.

For given hydrostatic pressure and geothermal gradient, the solute flux (1) reads:

$$J_{\mathrm{diff}} = \phi D \left[-\frac{dX^{(0)}(z)}{dz} + \beta \frac{X^{(0)}(z)}{z + T_{\mathrm{sf}}/G} \right], \qquad (5)$$

where

$$\beta = -\alpha + \frac{\tilde{M} g}{RG}. \qquad (6)$$

Eq. (5) with $\beta = 0$ corresponds to the Fickian diffusion law, $\vec{J}_{\mathrm{Fick}} = -\phi D \nabla X$, and β characterizes the *strength of non-Fickian part* of the solute flux. As the value of α is unknown, β is treated as a free parameter in our study.

3.1. Diffusive transport

First, we focus on purely diffusive transport without advection, which is reasonable for the following reasons: Firstly, for some geological systems the molecular diffusion is expected to be the dominant transport mechanism [*Haacke et al.*, 2008]. Secondly, advection is a well studied process; it is not influenced by the non-Fickian effects addressed here. In the saturated solution (the bubbly zone) advective and diffusive transports are merely summed.

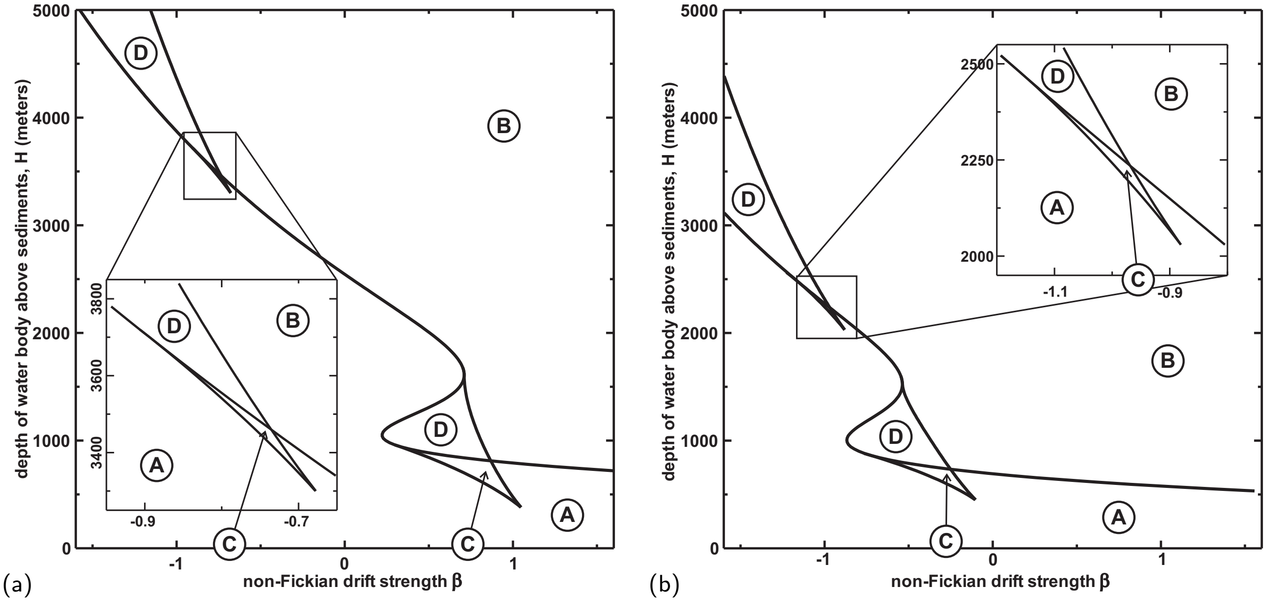

Figure 2. Diagram of diffusive methane transport regimes on the β–H plane (β quantifies the non-Fickian drift strength), in the seabed with methane bubbles, for the water-sediment interface temperature $T_{\rm sf} = 277\,K$. The geothermal gradient is $G = 40\,K/km$ (a) and $G = 60\,K/km$ (b). The profiles of solute flux J for 4 possible regimes (A, B, C, D) are plotted in Fig. 1.

We perform the following calculation: Employing Eq. (7) from the Appendix, we find the water–free-gas solubility profile for the temperature and pressure profiles given by Eq. (4) (such kind solubility profiles can be found in [*Haacke et al.*, 2008]). For the calculated solubility profile $X^{(0)}(z)$ and parameter β, Eq. (5) yields the profile of the diffusive flux $J(z)$. The variety of the solubility profiles for possible values of the temperature of the sediment-water interface $T_{\rm sf}$ and the depth of the water body above sediments H in combination with various strengths of non-Fickian drift β result in 4 classes of the flux profiles plotted in Fig. 1. According to Eq. (3), these flux profiles cause the production of free-gas mass $\dot{X}_{\rm b} = -(dJ/dz)$ for $\dot{X}_{\rm b} > 0$ or its depletion for $\dot{X}_{\rm b} < 0$.

We now discuss the diagrams of these regimes on the β–H plane. Fig. 2a shows the diagram of diffusive regimes in the system with geothermal gradient $G = 40\,K/km$. For shallow water bodies (small H), regime (A) occurs, with an upward diffusive flux near to the sediment-water interface, but a downward flux deeper within the sediments. As water depth increases, the flux inversion point shifts towards the sediment-water interface and finally disappears, so that the zone of downward diffusive methane flux covers the whole sediment volume, as shown in Fig. 1, regime (B). In regimes (A) and (B) all methane leaves the upper $2\,km$ layer of sediments either upwards, as identified locally in (A), or downwards, as in (B), and locally in (A). Intriguingly, besides regimes (A) and (B), there are regions where methane accumulation zones occur, caused by both upward diffusion (from below) and downward diffusion (from above). These zones may occur within the sediment column (C) and can touch the sediment-water interface (D). For $G = 40\,K/km$ this methane accumulation zone exists for non-Fickian drift strength β in range $[0.2, 1.1]$ in water bodies with depth between $0.5\,km$ and $1.5\,km$, and $\beta < -0.68$ in water bodies with depths greater than $3.2\,km$.

The regime diagram in Fig. 2a is plotted for a geothermal gradient $G = 40\,K/km$, which is typical for the Blake Ridge [*Paull et al.*, 2000; *Davie and Buffett*, 2001]. As G increases, regions (C) and (D), and the boundary between regions (A) and (B), shift to smaller depths and negative values of non-Fickian drift strength β. Fig. 2b presents the regime diagram for $G = 60\,K/km$, which is typical for the Cascadia margin [*Davie and Buffett*, 2003]. At sites with a low geothermal gradient, $G = 20\,K/km$, regime (A) prevails for water depths up to $5\,km$ (not illustrated).

Note, that the diagrams in Fig. 2 are constructed analysing the direction of flux $J_{\rm diff}$ within the sediment column. The sign of mass production $\dot{X}_{\rm b}$ is also affected by the nonuniformity of $\phi(z)$ (see Eqs. (3) and (5)). Importantly, the positive mass production zones, $\dot{X}_{\rm b} > 0$, in regimes (C) and (D) appear for any dependence $\phi(z)$. In the following subsection we calculate $\dot{X}_{\rm b}$, taking into account the presence of an upward fluid flow, as well as the nonuniformity of $\phi(z)$.

3.2. Impact of advection

Advective transport is more system-specific than diffusive flux; we need to additionally specify the dependence of the porosity ϕ on the vertical coordinate z, the sedimentation rate $v_{\rm s}(0)$, and the fluid filtration velocity $u_{\rm f}$. For the west Svalbard continental slope *Haacke et al.* [2008] adopted the dependence $\phi(z) = \phi(0)\exp(-z/L)$ with $\phi(0) = 0.555$ and $L = 1053\,m$. Sedimentation rate $v_{\rm s}(0) = 50\,cm/kyr$, geothermal gradient $G = 86.5\,K/km$, molecular diffusion coefficient $D = 2\cdot10^{-9}\,m^2/s$, and the upward fluid velocity assessed as $v_{\rm f}(0) = 0.1\,mm/yr$ have been used. Employing these parameters we calculated from Eq. (3) the free-gas mass production from the saturated aqueous solution. For a better understanding of the impact of advection the calculations have been performed not only for $v_{\rm f}(0) = 0.1\,mm/yr$, but also for smaller values of the upward fluid flux.

In Fig. 3 we plot the zones where methane is accumulated from the saturated solution into free-gas bubbles and the zones where free gas is dissolved. The lines demarcate the accumulation and dissolution zones for specified values of non-Fickian drift strength β. The former are observed for higher depths of water bodies next to the gas-hydrate

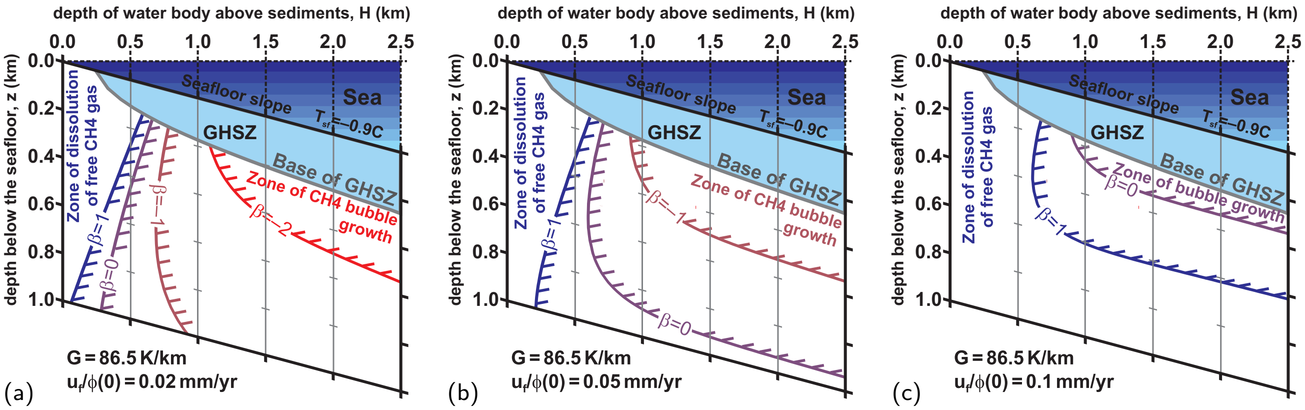

Figure 3. Boundaries between the zones of the growth of free-gas bubbles from the aqueous solution and the zones of dissolution of bubbles for different strength of non-Fickian drift β. The upward fluid flux $v_{\rm f}(0) = u_{\rm f}/\phi(0) = 0.02\,mm/yr$ (a), $v_{\rm f}(0) = 0.05\,mm/yr$ (b), and $v_{\rm f}(0) = 0.1\,mm/yr$ (c).

stability zone (GHSZ), and the latter occur under shallow water bodies. We wish to stress that the bubble growth (or dissolution) in the bubbly zone is a local process, which is not affected by the neighboring GHSZ (if any). This allows one to exclude the GHSZ from the explicit consideration. One can see that for a stronger advective flux $v_{\rm f}$, the accumulation zone shrinks and its existence requires bigger positive β. As one can see in Fig. 3, the non-Fickian correction to molecular diffusion remains rather important in the presence of advection.

3.3. Importance and uncertainties

The behavior described is considerably influenced by the non-Fickian drift of methane. We suggest that the Fickian diffusion law, which has been adopted in [*Davie and Buffett*, 2001] and its successors and corresponds to $\beta = 0$, should be modified.

The unresolved issue here is the specific value of β for methane. The authors are not aware of experimental data on thermodiffusion of methane in water, though there are a lot of experimental studies on the thermodiffusion of methane in mixtures of hydrocarbons (e.g. [*Wittko and Köhler*, 2005]). Theoretical studies (e.g. [*Semenov*, 2010]) provide formulae for calculation of the thermodiffusion constant from intermolecular potentials which are poorly established for water because of hydrogen bonds. We can only calculate $\tilde{M}g/RG = -0.725$ (for $G = 40\,K/km$), the isotope (*or* kinetic) part of the thermodiffusion [*Wittko and Köhler*, 2005; *Semenov*, 2010] $\alpha_{\rm isot} = (3/4)\ln(M^{\rm g}/N_1 M^{\rm host}) = -0.670$, and infer that the inter-molecule potential part $\alpha_{\rm potent}$ is positive (this qualitative conclusion is suggested by formulae in [*Semenov*, 2010]). Thus, $\beta^{\rm CH_4} < -0.055$ for aqueous solutions with geothermal gradient $G = 40\,K/km$, and $\beta^{\rm CH_4} < 0.187$ for $G = 60\,K/km$.

4. Implications for marine hydrates

The processes described above have major significance in relation to the occurrence of gas hydrate deposits. They suggest that in relatively shallow waters (area (A) in Fig. 2) the diffusive methane flux is directed upwards, into the GHSZ, while in deeper waters (area (B) in Fig. 2) methane diffuses downwards, leaving the GHSZ. In the former case the hydrate deposit capacity is enhanced, while in the latter, the deposit suffers diffusive depletion. The threshold sea depth, where the transition between these two regimes occurs, strongly depends on the non-Fickian drift strength β (which is a function of the thermodiffusion constant α and the geothermal gradient G). Nevertheless, theoretical assessment of the value of α suggests enhancements of hydrate deposits for the Cascadia margin and the Blake Ridge.

Another implication relates to the detection of marine methane hydrates. A very small amount (c. $1-2\%$) of gas bubbles is enough to change the sound speed in the sediment body and cause reflection of seismic waves; the reflecting layer is commonly referred to as the 'bottom simulating reflector' (BSR) (e.g. [*MacKay et al.*, 1994; *Hovland et al.*, 1999; *Paull et al.*, 2000]). It is typically assumed that the BSR marks the base of the GHSZ. Indeed, for an isothermal Fickian diffusion law, there are no reasons for the formation of a gaseous methane horizon (that may cut-across primary sedimentary features, such as bedding) other than the base of the GHSZ above which gas disappears having been transformed into hydrate. However, our theoretical findings suggest that commonly observed geothermal gradients are enough to explain the creation of gaseous methane horizons by thermodiffusion; formation of these horizons does not require the presence of the GHSZ or hydrates therein. This may be a reason why some BSRs seem to have no hydrate associated with them (e.g. [*Paull et al.*, 2000]). Rigorous quantitative prediction of appearance of BSRs without hydrates requires consideration of hydrate stability and will be presented in a separate publication. With the present work we conclude that within regions (C) and (D) in Fig. 2 conditions are favorable for the creation of potential BSRs that are generated by thermodiffusion processes alone, and are not linked to the boundary of a GHSZ at that depth. The Cascadia margin with $H = 1.3\,km$ and $G = 60\,K/km$ may well be close to regime (D) (Fig. 2b).

Our results suggest that some hydrate deposits may have no BSR at their base (as, for instance, reported by *Ecker et al.* [1998]; *Paull et al.* [2000]) because diffusion can lead to depletion of methane from the bubbly area as it does in regimes (A) and (B), which are most common (Fig. 2). In this case, only the balance between the sedimentation rate (which provides a flux of methane mass from the GHSZ to the underlying free-gas zone) and the diffusive depletion rate determines whether the BSR appears. In areas with higher sedimentation rates it may be that BSRs will be more common. This relationship should be addressed in future modelling, involving consideration of methane-hydrate stability and sedimentation processes (as in [*Davie and Buffett*, 2001], but taking account of the non-Fickian effects in diffusion).

5. Conclusion

We have theoretically explored the process of diffusive migration of aqueous methane in the presence of bubbles, when they are immovably trapped by a porous matrix—as occurs commonly in seafloor sediments, swamps, or terrestrial aquifers. The effect of temperature inhomogeneity across the system (geothermal gradient) and gravitational force have been accounted for.

Non-Fickian corrections—thermodiffusion and gravitational buoyancy—appear to play an important role in the migration of methane in sediments in deep-water settings. They can assist the formation of a methane accumulation zone in the upper part of the sediment column under water bodies with depths in range $0.5-1.5\,km$ and the very deep ones (Fig. 2). For the latter the minimal depth required depends on the geothermal gradient G: it is around $3.2\,km$ for $G=40\,K/km$ (such G is typical for the Blake Ridge) and $2.2\,km$ for $G=60\,K/km$ (such a G is typical for the Cascadia margin).

Under moderately deep water bodies, gas hydrate deposits should be enhanced (presumably, as for the Cascadia margin and the Blake Ridge), and conversely, under deep water bodies gas hydrate deposits should be subject to a stronger diffusive depletion than with the purely Fickian diffusion. The depth of transition between these two regimes increases with decrease of the geothermal gradient G: this is the reason why the relatively deep Blake Ridge with $G\approx 40\,K/km$ and the shallower Cascadia margin with large $G\approx 60\,K/km$ appear to have similar conditions for the formation of gaseous methane accumulation zones.

It is a consequence of our results, that the effects of non-Fickian diffusion remain rather important even in the presence of advective transport. For instance, Fig. 3 illustrates that, depending on β and for conditions of the west Svalbard continental slope [*Haacke et al.*, 2008], non-Fickian diffusion can either extend or shrink the zone of methane accumulation from solution into bubbles.

Remarkably, the early theoretical study [*Xu and Ruppel*, 1999] on the formation of natural methane hydrate deposits had inferred that these systems should be advection dominated; this was needed to explain the enhancement of hydrate deposit capacity. Later on, *Haacke et al.* [2008] reported a case study from the west Svalbard continental slope, where the formation of a persistent free-gas zone below the gas hydrate stability zone required the system to be diffusion dominated. These studies have adopted the Fickian diffusion law. In our study we see that the actual, non-Fickian diffusion, even for negligible advection, can lead both to the enhancement of hydrate deposits and the formation of a persistent free-gas zone.

Unfortunately, we cannot determine precise values for the thermodiffusion constant of aqueous solutions of methane from the literature, and can only rely on theoretical predictions (e.g. [*Semenov*, 2010]), to estimate their values, as we do here. Our findings highlight the necessity of experimental determinations of the thermodiffusion constant for aqueous methane solutions.

Acknowledgments. The authors are grateful to A. Gorban and D. V. Lyubimov for fruitful discussions and comments. The work has been supported by NERC Grant no. NE/F021941/1. This paper is published with the permission of the Director of the British Geological Survey.

Appendix: Methane solubility

For theoretical evaluation of the methane solubility at equilibrium with the vapor phase, we employ the scaled particle theory [*Pierotti*, 1976] and the Van der Waals' real gas model (see [*Goldobin and Brilliantov*, 2011] for mathematical details). These yield

$$X^{(0)}=\frac{(1-Y)\,v_{\mathrm{liq}}n}{1-nb}\exp\left[-\frac{G_c+G_i}{RT}-\frac{2an}{RT}+\frac{nb}{1-nb}\right].\quad(7)$$

Here G_c is the enthalpy of formation of the cavities for one mole of solute molecules,

$$\begin{aligned}\frac{G_c}{RT} &= -\ln(1-y)+\frac{3y}{1-y}\frac{\sigma_{\mathrm{g}}}{\sigma_{\mathrm{liq}}}\\ &\quad+\left[\frac{3y}{1-y}+\frac{9}{2}\left(\frac{y}{1-y}\right)^2\right]\left(\frac{\sigma_{\mathrm{g}}}{\sigma_{\mathrm{liq}}}\right)^2+\frac{\pi\sigma_{\mathrm{g}}^3N_{\mathrm{A}}P}{6RT},\end{aligned}$$

the effective diameter of water molecules $\sigma_{\mathrm{liq}}=2.77\,\mathring{A}$, the one for methane $\sigma_{\mathrm{g}}=3.27\,\mathring{A}$; $y=(\pi/6)n_{\mathrm{liq}}\sigma_{\mathrm{liq}}^3$ (at standard conditions, $y_{\mathrm{H_2O}}=0.371$, the corresponding molar volume of liquid water $v_{\mathrm{liq}}=17.95\,cm^3/mol$ [*Pierotti*, 1976]); Avagadro's number $N_{\mathrm{A}}=6.02\cdot 10^{23}$. The molar density $n(T,P)$ of gaseous methane can be determined from the Van der Waals equation of state

$$P=nRT/(1-nb)-an^2$$

with $a=0.2283\,m^6Pa/mol^2$ and $b=4.278\cdot 10^{-5}m^3/mol$, which has unique analytical solution with respect to n for $T>190\,K$ (the expression for this solution is lengthy though can be provided by any package for analytical computations, such as Maple). The molar enthalpy of interaction of methane molecule with the surrounding water molecules, G_i, is nearly temperature independent, $G_i/R\approx -1138\,K$.

The molar fraction of water in the vapor phase

$$\begin{aligned}Y^{\mathrm{H_2O}}=\frac{P_0}{P}\left(\frac{T}{T_0}\right)^{\frac{\Delta c_P^{\mathrm{H_2O}}}{R}}\exp&\left[\frac{v_{\mathrm{liq}}(P-P_0)}{RT}\right.\\ &\left.-\frac{\Delta h_0^{\mathrm{H_2O}}-\Delta c_P^{\mathrm{H_2O}}T_0}{R}\left(\frac{1}{T}-\frac{1}{T_0}\right)\right],\end{aligned}\quad(8)$$

where the difference between the molar specific heat capacity of liquid water and steam $\Delta c_P^{\mathrm{H_2O}}/R=-5.00$, the molar enthalpy of vaporization $\Delta h_0^{\mathrm{H_2O}}/R=4890\,K$ at $T_0=373\,K$ and $P_0=1\,atm$. Thus, one has all ingredients for calculation of the solubility $X^{(0)}(T,P)$ with Eq. (7).

Notation

a, b	Van der Waals' constants, $\mathrm{Pa\,m^6/mol^2}$ and $\mathrm{m^3/mol}$, respectively.
D	molecular diffusion coefficient, $\mathrm{m^2/s}$.
G	geothermal gradient, K/m.
$\vec{g}$	gravity, $\mathrm{m/s^2}$.
G_c	enthalpy of formation of the cavities in the solution for one mole of the solute molecules, J/mol.
G_i	enthalpy of interaction of the solute molecule with the solvent molecules, per one mole of the former, J/mol.
H	depth of the water body above sediments, m.
$\vec{J}$	diffusive flux of the CH_4 molar fraction, m/s.
$\tilde{M}$	effective molar mass of methane, $\tilde{M}=M_{\mathrm{CH_4}}-N_1M_{\mathrm{H_2O}}$, where N_1 is the number of the water molecules replaced by the methane molecule in the solution; $\tilde{M}=-0.0243\,\mathrm{kg/mol}$.

n	the molar density of gaseous methane, mol/m^3.
P, P_0	pressure and the atmospheric pressure, respectively, Pa.
R	universal gas constant, 8.31 J/(mol K).
T, $T_{\rm sf}$	temperature and the sediment-water interface temperature, respectively, K.
$u_{\rm f}$	filtration velocity of fluid, m/s.
$v_{\rm f}$	interstitial fluid velocity, $u_{\rm f} = \phi v_{\rm f}$, m/s.
$v_{\rm liq}$	molar volume of liquid water, m^3/mol.
X, $X^{(0)}$	molar fraction of CH$_4$ in aqueous solution and the solubility, respectively, dimensionless.
X_b	molar fraction of gaseous methane in bubbly fluid, dimensionless.
Y	molar fraction of water in the methane bubble, dimensionless.
z	depth in sediments, below the sediment-water interface, m.
α	thermodiffusion constant, dimensionless; Soret coefficient $S_T = \alpha/T$.
β	$= -\alpha + \tilde{M}g/RG$ characterizes the non-Fickian drift strength, dimensionless.
$\phi(z)$	porosity of sediments, dimensionless.
$\rho_{\rm liq}$	density of liquid water, kg/m^3.
BSR	bottom simulating reflector.
GHSZ	gas hydrate stability zone.

References

Algar, C. K., B. P. Boudreau, and M. A. Barry, Initial rise of bubbles in cohesive sediments by a process of viscoelastic fracture, *J. Geophys. Res.*, *116*, B04207, 2011.

Archer, D., Methane hydrate stability and anthropogenic climate change, *Biogeosciences*, *4*, 521–544, 2007.

Barry, M. A., B. P. Boudreau, B. D. Johnson, and A. H. Reed, First-order description of the mechanical fracture behavior of fine-grained surficial marine sediments during gas bubble growth, *J. Geophys. Res.*, *115*, F04029, 2010.

Bernard, R. A., and R. H. Wilhelm, Turbulent diffusion in fixed beds of packed solids, *Chem. Eng. Prog.*, *46*, 233–244, 1950.

Bird, R. B., W. E. Stewart, and E. N. Lightfoot, *Transport Phenomena*, 2 ed., Wiley, 2007.

Davie, M. K., and B. A. Buffett, A numerical model for the formation of gas hydrate below the seafloor, *J. Geophys. Res.*, *106*, 497–514, 2001.

Davie, M. K., and B. A. Buffett, Sources of methane for marine gas hydrate: inferences from a comparison of observations and numerical models, *Earth Planet. Sci. Lett.*, *206*, 51–63, 2003.

Donaldson, J. H., J. D. Istok, M. D. Humphrey, K. T. O'Reilly, C. A. Hawelka, and D. H. Mohr, Development and testing of a kinetic model for oxygen transport in porous media in the presence of trapped gas, *Ground Water*, *35*, 270–279, 1997.

Ecker, C., J. Dvorkin, and A. Nur, Estimating the amount of hydrate and free gas from surface seismic, *SEG Technical Program Expanded Abstracts*, *17*, 566–569, 1998.

Garg, S. K., J. W. Pritchett, A. Katoh, K. Baba, and T. Fujii, A mathematical model for the formation and dissociation of methane hydrates in the marine environment, *J. Geophys. Res.*, *113*, B01201, 2008.

Goldobin, D. S., and N. V. Brilliantov, Diffusive Counter Dispersion of Mass in Bubbly Media, *E-print arxiv:1011.5140*, 2011. url: http://arxiv.org/abs/1011.5140

Haacke, R. R., G. K. Westbrook, and M. S. Riley, Controls on the formation and stability of gas hydrate-related bottom-simulating reflectors (BSRs): A case study from the west Svalbard continental slope, *J. Geophys. Res.*, *113*, 2008.

Hnedkovsky, L., R. H. Wood, and V. Majer, Volumes of aqueous solutions of CH4, CO2, H2S and NH3 at temperatures from 298.15 K to 705 K and pressures to 35 MPa, *J. Chem. Thermodyn.*, *28*, 125–142, 1996.

Hovland, M., T. J. G. Francis, G. E. Claypool, and M. M. Ball, Strategy for scientific drilling of marine gas hydrates, *JOIDES Journal*, *25*, 20–24, 1999.

Kayen, R. E., and H. J. Lee, Pleistocene slope instability of gas hydrate-laden sediment on the Beaufort Sea margin, *Marine Geotechnology*, *10*, 125–141, 1991.

Lyubimov, D. V., S. Shklyaev, T. P. Lyubimova, and O. Zikanov, Instability of a drop moving in a brinkman porous medium, *Phys. Fluids*, *21*, 014105, 2009.

MacKay, M. E., R. D. Jarrard, G. K. Westbrook, and R. D. Hyndman, Origin of bottom-simulating reflectors: Geophysical evidence from the Cascadia accretionary prism, *Geology*, *22*, 459–462, 1994.

Paull, C. K., R. Matsumoto, P. J. Wallace, and W. P. Dillon (Eds.), *Proceedings of the Ocean Drilling Program, Scientific Results*, vol. 164, College Station, TX (Ocean Drilling Program), 2000.

Pierotti, R. A., A scaled particle theory of aqueous and nonaqueous solutions, *Chemic. Rev.*, *76*, 717–726, 1976.

Richter, J., Evidence for significance of other-than-normal diffusion transport in soil gas exchange, *Geoderma*, *8*, 95–101, 1972.

Semenov, S. N., Statistical thermodynamic expression for the soret coefficient, *Europhys. Lett.)*, *90*, 56002, 2010.

Sorét, C., Sur l'état d'équilibre que prend, au point de vue de sa concentration, une dissolution saaline primitivement homogène, dont deux parties sont portées à des températures différentes, *Archives des Sciences Physiques et Naturelles de Genève*, *2*, 48–61, 1879.

Wittko, G., and W. Köhler, Universal isotope effect in thermal diffusion of mixtures containing cyclohexane and cyclohexane-d[sub 12], *J. Chem. Phys.*, *123*, 014506, 2005.

Xu, W. Y., and C. Ruppel, Predicting the occurrence, distribution, and evolution of methane gas hydrate in porous marine sediments, *J. Geophys. Res.*, *104*, 5081–5095, 1999.

D. S. Goldobin, N. V. Brilliantov, and J. Levesley, Department of Mathematics, University of Leicester, Leicester LE1 7RH, UK. (Denis.Goldobin@gmail.com)

M. A. Lovell, Department of Geology, University of Leicester, Leicester LE1 7RH, UK.

C. A. Rochelle, P. D. Jackson, and J. G. Rees, British Geological Survey, Keyworth, Nottingham NG12 5GG, UK.

A. M. Haywood and S. J. Hunter, School of Earth and Environment, University of Leeds, Leeds LS2 9JT, UK.